IOPscience iopscience.iop.org

Home Search Collections Journals About Contact us My IOPscience

Structural coherence between phases in $Ni_{0.35}Ag_{0.65}$ thin films

This article has been downloaded from IOPscience. Please scroll down to see the full text article.

2000 J. Phys.: Condens. Matter 12 3939

(http://iopscience.iop.org/0953-8984/12/17/302)

View the table of contents for this issue, or go to the journal homepage for more

Download details:
IP Address: 171.66.16.221
The article was downloaded on 16/05/2010 at 04:51

Please note that terms and conditions apply.

J. Phys.: Condens. Matter **12** (2000) 3939–3953. Printed in the UK PII: S0953-8984(00)11017-3

Structural coherence between phases in $Ni_{0.35}Ag_{0.65}$ thin films

O Proux†, J Mimault‡, J R Regnard†§, C Revenant-Brizard†, B Mevel† and B Dieny‖

† CEA/Grenoble, Département de Recherche Fondamentale sur la Matière Condensée, SP2M/IRS¶, 17 rue des Martyrs, F-38054 Grenoble Cédex 9, France
‡ Laboratoire de Métallurgie Physique, UMR CNRS 6630, SP2MI, Boulevard 3, Téléport 2, BP 179, F-86960 Futuroscope Cédex, France
§ Université Joseph Fourier, BP 53 X, F-38041 Grenoble Cédex, France
‖ CEA/Grenoble, Département de Recherche Fondamentale sur la Matière Condensée, SP2M/NM, 17 rue des Martyrs, F-38054 Grenoble Cédex 9, France

Received 14 January 2000, in final form 14 March 2000

Abstract. $Ni_{0.35}Ag_{0.65}$ thin films were studied by means of both x-ray absorption spectroscopy and x-ray diffraction, in the as-deposited and annealed states. Short-range-order investigation has established that nickel atoms are either clustered in small pure Ni aggregates or dispersed in an Ag-rich solid solution. For the as-deposited and 250 °C annealed samples, an accurate interpretation of the diffraction spectra requires one to take into account a degree of structural coherence between these two phases, which are preferentially oriented with the dense planes parallel to the surface. Local order and long-range-order characterizations then give coherent results. The mean size of the pure Ni aggregates increases from approximately 1 nm in the as-deposited state to 3–5 nm after a 400 °C anneal. The maximum Ni solubility in the Ag matrix was estimated to be around 7 at.% for these samples. All of the reported results—the natures of the various phases, and mean sizes, shapes and orientations of the aggregates—are discussed with regard to the other structural (extended x-ray absorption fine-structure, anomalous small-angle x-ray scattering) and magnetic information.

1. Introduction

The discovery of giant magnetoresistance (GMR) in magnetic heterogeneous alloys [1, 2] has stimulated great interest in their preparation, characterization and physical properties. These alloys are prepared from two immiscible materials. They consist of ferromagnetic aggregates embedded in a non-magnetic metallic matrix. Understanding quantitatively the GMR in such materials requires a good knowledge of their nanostructure: crystallographic structure, mean size of the various aggregates, as well as the correlation distance between them. Usually, these alloys are produced by codeposition of the two elements onto a substrate. According to the substrate temperature during deposition and to subsequent anneals, the deposited film may be formed either as a homogeneous supersaturated solid solution or as a totally demixed material or a heterogeneous alloy.

In the present paper, we report structural investigations performed on as-deposited and annealed $Ni_{0.35}Ag_{0.65}$ sputtered thin films. The magnetic and transport properties of these films have been investigated previously [3]. The particular interest in these studies is that the magnetic properties of the nickel aggregates strongly depend on their size. Indeed, in Ni/Ag

¶ Laboratory associated with Université Joseph Fourier de Grenoble, France.

0953-8984/00/173939+15$30.00 © 2000 IOP Publishing Ltd

multilayers, it was observed that the Curie temperature of the Ni layers drops strongly below room temperature for Ni layer thickness below ∼12 Å [4]. Similarly, for nanometre-scale Ni aggregates, the magnetic ordering temperature within each grain depends on its size. Therefore, both intragrain and intergrain magnetic fluctuations must be considered in the interpretation of the magnetic properties of NiAg alloys. For the particular Ni concentration $x = 0.35$, the GMR amplitude does not change between the as-deposited state and the state after annealing at 250 °C for ten minutes (at 30 K and 4 T; $\Delta R/R \sim 4\%$) but decreases upon the 400 °C annealing ($\Delta R/R \sim 0.8\%$ in the same conditions). Two contributions generate the GMR effect: the spin-disorder and the spin-valve magnetoresistance (SDMR and SVMR). The first of these, responsible for the high-field MR response, is associated with very small magnetic aggregates and with interfacial magnetic fluctuations. The second, which gives the MR variation at low field, is due to the change in the relative orientation of the magnetization in neighbouring magnetic aggregates.

Various experiments reported in the literature indicate that NiAg solid solutions can be obtained, especially for low concentration of one element, even if the systems have a positive heat of mixing ($\Delta H_{\mathrm{mix}} = +15$ kJ mol^{-1}) [5]. Production methods include for example mechanical alloying [6], the gas condensation method leading to powder [7, 8], ion beam mixing of multilayers [9], condensation onto a substrate by co-evaporation of the two elements produced by an electron beam [10], laser ablation [11], sputtering [12] and magnetron sputtering [13, 14]. A post-annealing process allows the creation of heterogeneous Ni–Ag alloys, but such structural states have already been produced in as-deposited layers by molecular beam epitaxy [15] and by magnetron sputtering, for atomic nickel concentrations ranging from 0.20 to 0.35 [13, 14, 16].

X-ray diffraction (XRD) investigation is a standard method for identifying the various phases present in a material and estimating the size of the coherent diffracting domains. Frequently, the lattice parameter of each phase, determined from this long-range-order investigation, is plotted versus the mean composition of the sample: a continuous evolution of such a parameter (a Vegard law dependence) is attributed to the presence of a solid solution in the material analysed. Nevertheless, no information about the homogeneity of this solid solution can be obtained from this simple analysis, and a short-range study of the neighbourhood of each element in this phase has to be performed, by x-ray absorption spectroscopy (XAS) for example [17]. The lack of the series of reflections associated with interplanar distances of the pure element does not prove the existence of an alloy phase: experimental evidence that such an interpretation may be erroneous has already been obtained for two binary systems, Cu–Co [18] and Au–Pt [19].

The aim of the present study is to investigate in more detail the nanostructure of the $Ni_{0.35}Ag_{0.65}$ alloys and to correlate it with the magneto-transport properties. Analysis of the long-range-order experiments performed by means of XRD was carried out in parallel with the short-range-order investigation by XAS. We also compare the mean size and the shape of the nickel aggregates obtained to those estimated from XAS [14] and from anomalous small-angle x-ray scattering (ASAXS) [16].

2. Experimental details

2.1. Sample preparation

Samples were prepared by simultaneous DC-magnetron sputtering of Ni and Ag onto glass substrates. This amorphous substrate, maintained at liquid nitrogen temperature during deposition, does not induce *a priori* any preferential orientation of the crystallites. The

composition of the alloy films was adjusted by varying the deposition rates of both components. The total thickness of the film was approximately 200 nm. The mean deposition rate was about 25 nm min^{-1}. The base pressure was 2×10^{-8} Torr and the argon pressure was 3×10^{-3} Torr during deposition. Anneals were performed in a high-vacuum furnace (10^{-6} Torr), for ten minutes, at $T_A = 250$ °C and 400 °C.

2.2. Extended x-ray absorption fine-structure measurements

Measurements were performed on the EXAFS 1 station at the LURE-DCI synchrotron (Orsay, France) operating at 1.85 GeV at the Ni K edge (8.333 keV), using a (331) Si channel-cut monochromator. Acquisitions of the extended x-ray absorption fine-structure (EXAFS) signal were carried out by detection of the conversion-electron yield, in order to obtain depth-limited information. Other studies [20, 21] allow one to estimate such a depth to be around 50 nm. Furthermore, acquisitions were performed at liquid nitrogen temperature [22] to obtain a better-defined signal over an enlarged energy range, due to the reduction of the thermal damping of the oscillations.

All spectra were analysed using the same standard procedure. Edge energy was determined at the first inflexion point in the edge region. The base-lines were fitted with polynomials, a first-order one for the pre-edge and a fifth-order one after the edge. The EXAFS data were Fourier transformed using a Hanning window from 3 to 13 $Å^{-1}$ and a k^3-weighting. Filtering of the first coordination shells was performed by inverse Fourier transformation from 1.7 to 3.1 Å.

The fitting process was carried out using the theoretical amplitude [23] in the single-scattering approximation [24], with four parameters for each shell around the central atom: the nature and the number of neighbours (N), the mean square relative displacement (MSRD, σ), the correlation distance (R) and the shift of the threshold energy (ΔE_0), the number of independent points [25] being estimated to be 12. The function minimized during this fitting operation was

$$\Phi = \left(\sum k^2 \left[\chi_{\mathrm{exp}}(k) - \chi_{\mathrm{th}}(k)\right]^2\right) \Big/ \left(\sum k^2 \chi^2_{\mathrm{exp}}(k)\right) \tag{1}$$

where $\chi_{\mathrm{exp}}(k)$ and $\chi_{\mathrm{th}}(k)$ are the experimental and the corresponding fit points; a typical value of ϕ was 2.5×10^{-2}. As the nearest-neighbour coordination number N is highly correlated with σ, an accurate determination of N needs to be performed in the (N, σ) space. The error on N can then be estimated by calculating numerical values of the ϕ-function for different pairs (N, σ) [26]. Contours of this ϕ-function are plotted at different numerical values, defined in terms of ϕ_{min} (the minimum of the function) as ϕ_{min}/C, where C is a constant. As an example, such curves are plotted in figure 1 for different values of C running from 95% to 60%: the contours are inclined ellipses. The uncertainty in a given parameter is then estimated by projecting the extremum of the particular curve obtained for $C = 95\%$ on the corresponding axis. The uncertainty in the nearest-neighbour (NN) coordination number is estimated to be around 0.4 for the Ni–Ni bonds and 1 for the Ni–Ag ones. The uncertainty in the absolute distance R is 0.002 nm and that in the MSRD σ is about 5×10^{-4} nm.

EXAFS studies of nanostructured materials often show a decrease of the amplitude of the oscillations, attributed to an increase of the interface-to-bulk ratio. Such a size effect leads to a decrease in the mean coordination number (N) for the first shells [26], surface cluster atoms having a strongly modified environment with respect to the core atoms, which have a complete environment (coordination number equal to that of the reference, N_{ref}). The binary alloys studied can present three types of bond around central Ni atoms: Ni–Ni bonds (N_{core}) due to Ni atoms completely embedded in pure Ni clusters, Ni–Ag bonds typical of interfaces between the Ni clusters and the Ag matrix ($N_{\mathrm{interface}}$) and Ni–Ag bonds due to Ni atoms inserted

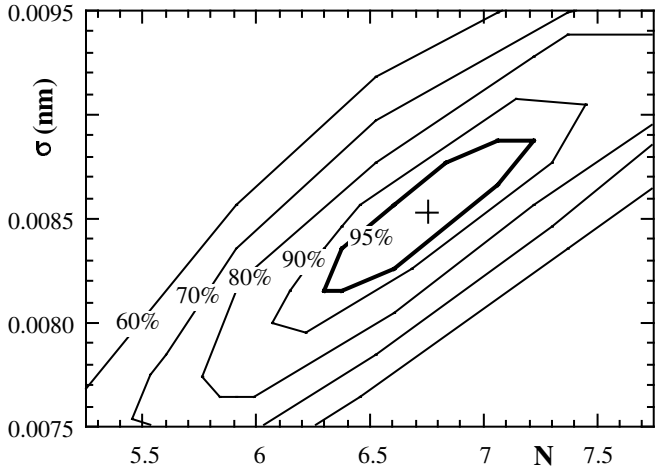

Figure 1. A contour plot of the ϕ-function minimized in the fits performed as a function of the Ni–Ni coordination number and the MSRD σ (in nanometres), relative to the first-shell analysis of the as-deposited $Ni_{0.35}Ag_{0.65}$ film.

in the Ag matrix (N_{matrix}). For Ni face-centred cubic (FCC) structure, N_{ref} is equal to 12, so one can write

$$N_{\text{core}} + N_{\text{interface}} + N_{\text{matrix}} = 12. \tag{2}$$

Due to the local scale incoherence at the cluster–matrix interface, which induced a very large distance distribution of Ni–Ag bond lengths (large $\sigma_{\text{interface}}$), EXAFS oscillations linked to $N_{\text{interface}}$ have a very much reduced weight in the total $\chi(k)$ EXAFS signal. We consider its contribution as quasi-negligible for this kind of film and the sum of the calculated experimental nearest neighbours is then lower than 12.

From these results, one can determine the ratio of Ni atoms being substituted in the Ag matrix ($F_{\text{Ni/Ag}} = N_{\text{matrix}}/12$) and the complementary value, the ratio of Ni atoms either agglomerating in pure TM clusters or at the interface (F_{clusters}). The difference between N_{core} and the reference Ni–Ni coordination number N_{ref} (weighted by F_{clusters} if Ni atoms are both in Ni clusters and in the Ag matrix [14]) allows one to characterize the surface-to-volume ratio of the clusters. By assuming the FCC clusters to be spherical, a simple model [27] allows one then to determine the mean diameter D of the clusters from these values:

$$D = 1.06\,a\,\frac{F_{\text{clusters}}N_{\text{ref}}}{F_{\text{clusters}}N_{\text{ref}} - N_{\text{clusters}}} \tag{3}$$

where a is the lattice parameter of the FCC structure.

In XRD analysis, the particle size is generally estimated by the coherence length, a parameter related to the mean thickness of the diffracting objects, in the direction perpendicular to the surface for a θ–2θ geometry. A spherical particle of diameter D yields a scattering very similar to that of a cubic entity of the same volume. Hence, one can define for spherical particles an equivalent coherence length L by [14]

$$L \approx 0.8\,D. \tag{4}$$

The uncertainty in the determination of this value can be determined from equations (3) and (4):

$$\frac{\Delta D}{D} = \frac{\Delta L}{L} = \frac{\Delta(F_{\text{clusters}}N_{\text{ref}} - N_{\text{clusters}})}{F_{\text{clusters}}N_{\text{ref}} - N_{\text{clusters}}}. \tag{5}$$

As ΔL is inversely proportional to $F_{\text{clusters}}N_{\text{ref}} - N_{\text{clusters}}$, the evaluation of L is only significant for small particles (high values of $N_C - N$); typically $L < 2.5$ nm.

2.3. X-ray diffraction measurements

Room temperature XRD patterns were collected using Cu Kα radiation with a commercial Siemens D500 powder diffractometer in the symmetric geometry (θ–2θ) and a home-built diffractometer [28] used in the dispersed mode and asymmetric geometry (α–2θ) in order to obtain a rocking curve.

θ–2θ scans were recorded with a step size of 0.02° (for the 2θ angle) and a count time of 10 s for each step, in order to obtain spectra with a high signal-to-noise ratio.

α–2θ scans were recorded with a linear detector (step size: 0.0455°) of opening window 20° and a count time of 100 s per scan. θ_B is the Bragg angle, for a given reflection of the incident beam by atomic planes parallel to the surface, and α the incidence angle of the beam with respect to the surface. For each angle $\psi = \theta_B - \alpha$, the integrated intensity of the (111) peak was calculated, in order to determine the experimental rocking curve $I(\psi)$ for this particular reflection.

Analysis of the θ–2θ scans was carried out in the reciprocal space, and intensity is reported in relation to the parameter s equal to $2(\sin\theta)/\lambda$, where θ is the angle between the incident x-ray beam and the film surface, and λ the x-ray wavelength ($\lambda = 0.1506$ nm). Ni and Ag powders were used as 'standards' to correct d-spacing systematic errors and to estimate the instrumental broadening. The profiles of the XRD peaks were analysed using the Warren–Averbach method [29] in order to separate the effects of the mean size L_W, due to spatially limited coherently diffracting domains, from those caused by microstrains. Nevertheless, such a sophisticated analysis is only applicable to the Ag-rich-phase crystallites, since nickel atoms are in a minority, and also have a small diffracting power compared to the silver ones.

3. EXAFS results

Simulations were performed on the filtered EXAFS signal for two different bonds: Ni–Ni, characteristic of nickel agglomerated in pure nickel aggregates, and Ni–Ag, characteristic of nickel atoms embedded in the Ag-rich matrix. Values determined from these simulations are reported in table 1. Considering the uncertainties, the present values are in good agreement with those obtained using the EXCURV92 spherical-wave X_α model [32] published in a previous paper [13]. They can therefore be considered with confidence.

Table 1. Fit results for the filtered EXAFS spectrum for the $Ni_{0.35}Ag_{0.65}$ alloys as deposited and annealed at 250 and 400 °C. The parameter N is the NN coordination number, σ the Debye–Waller factor and R the NN coordination distance. Filtering was performed to take into account both Ni–Ni and Ni–Ag contributions. For comparison: for pure Ni: $N = 12$, $R = 0.248$ nm, $\sigma = 0.006$ nm. $D_{\text{Ni,XAS}}$ is the diameter of the pure nickel aggregates estimated from the results of the EXAFS spectra simulations and $L_{\text{Ni,XAS}}$ the equivalent corresponding coherence length.

Samples:	As deposited			250 °C			400 °C		
Bonds	N	σ (nm)	R (nm)	N	σ (nm)	R (nm)	N	σ (nm)	R (nm)
Ni–Ni	6.7	0.0085	0.247	8.6	0.008	0.248	11.3	0.007	0.248
Ni–Ag	2	0.011	0.275	2	0.010	0.274			
$D_{\text{Ni,XAS}}$ (nm)		1.1 ± 0.4			2.5 ± 1			6 ± 4	
$L_{\text{Ni,XAS}}$ (nm)		0.9 ± 0.3			2.0 ± 0.8			5 ± 3	

Even for the as-deposited state, the Ni–Ni distance is close to that of bulk metallic nickel. The MSRD term $\sigma_{\mathrm{Ni-Ni}}$ is larger than that of the reference sample, and decreases with the annealing treatments. This behaviour reflects a substantial disorder in the neighbourhood of the central nickel atoms surrounded by other nickel atoms in the as-deposited sample. Simultaneously, the number of neighbours increases from 6.7 (as-deposited sample) to 11.3 (400 °C annealing), a value close to that for the reference.

The number of Ni–Ag bonds, equal to 2, remains unchanged in the as-deposited and 250 °C anneal states. It vanishes to 0 after annealing at 400 °C and we consider that all the nickel atoms are out of the silver matrix.

From the number of nearest Ni–Ni neighbours, the diameter of the nickel aggregates (equation (3)) and the equivalent coherence length (equation (4)) can be estimated (table 1). The mean coherence length of the as-deposited aggregates is thus estimated to be 1 nm. It increases after the first annealing treatment (250 °C) to 2.0 nm and after the second one (400 °C) to 5 nm.

4. XRD results

4.1. Symmetric geometry (θ–2θ)

Figures 2 display the experimental XRD patterns, limited to the reciprocal-lattice area near the Ag(111) and Ni(111) reflections (figure 2(a)) and near the Ag(311) and Ag(222) ones (figure 2(b)).

For each sample studied, two peaks associated with the reflection on planes of the same family $\{hhh\}$ can be clearly observed and are attributed to an Ag-rich phase. These peaks have been extensively studied in a previous work [14], which has allowed the estimation of the atomic concentration of nickel inserted in this silver matrix, the coherence length of the silver-rich crystallites (around 4 nm for the as-deposited and 250 °C annealed samples, 7.5 nm for the 400 °C annealed one) and the microstrain ratio.

Furthermore, the XRD patterns display a small and broad peak, located between the peaks of the (111) dense planes of 'pure' FCC Ag and Ni (figure 2(a)). With the annealing process, the position of the bottom of this peak evolves in the reciprocal space and reaches a value close to that of the position of the bulk Ni(111) reflection for the 400 °C annealed material. This reflection can be unambiguously distinguished from the (200) reflection of the Ag-rich phase (which would be located at a larger distance in reciprocal space than the Ag(200) reflection).

The usual analysis consists in calculating such XRD patterns by summing over two independent peaks: the scattered intensity is assumed to be coming from two nanocrystalline phases in complete structural incoherence. Such a simulation can be performed with diffraction profiles of pseudo-Voigt types [33]. It leads to the determination of two different natures of crystallites: Ag-rich and Ni-rich phases. The lattice parameter is found to reach 0.37 nm for the Ni-rich phase in the as-deposited state, leading to an atomic composition of silver atoms around 35% obtained by applying the Vegard law. Anyway, such a hypothesis is incompatible with the local atomic environment indicated by the EXAFS for the as-deposited and 250 °C annealed thin films: Ni atoms present either in the Ag-rich phase or in 'pure' Ni aggregates.

Annealing performed on solid solutions with positive heat of mixing often results in a decomposition of these metastable phases. Such decomposition originates from either a spinodal mechanism or a nucleation–growth process of thermodynamically stable crystallites. The continuous appearance of these new phases can result in there being small inhomogeneities, taking the form of very thin particles appearing quasi-periodically and partially in coherence with the matrix. A transmission electron microscopy (TEM) investigation performed on

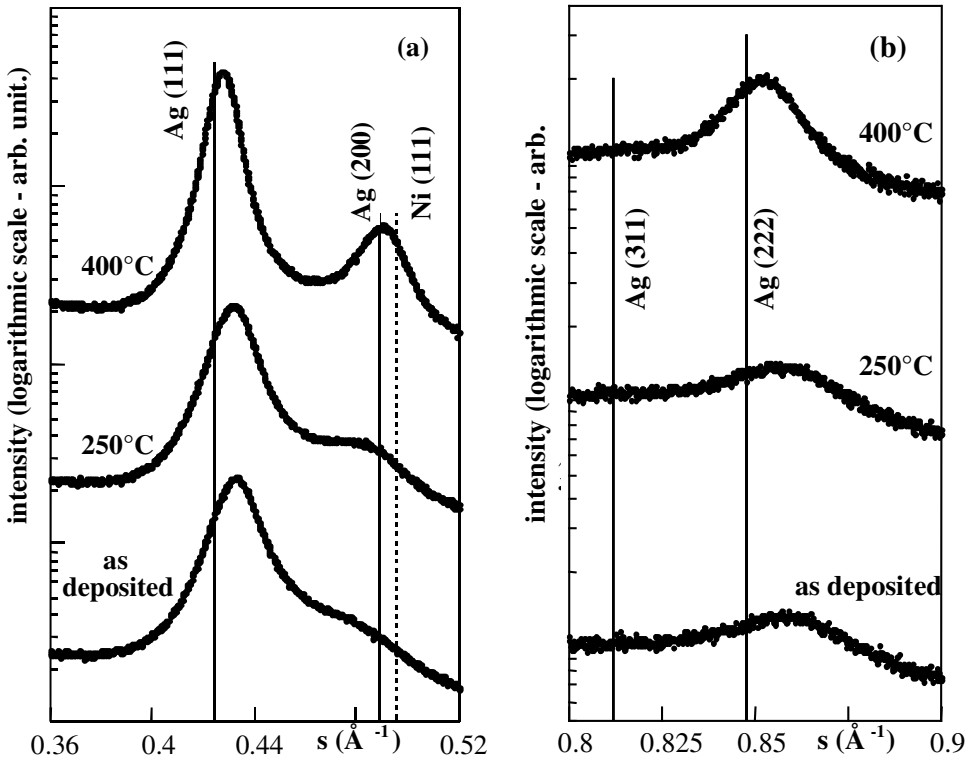

Figure 2. XRD patterns of the as-deposited and 250, 400 °C annealed $Ni_{0.35}Ag_{0.65}$ alloys limited to the reciprocal-lattice areas near and between the theoretical reflections Ag(111) and Ni(111) (a) and the theoretical reflections Ag(311) and Ag(222) (b).

$(Ni_{80}Fe_{20})_{0.4}Ag_{0.6}$ sputtered films has revealed a coherent integration of the NiFe particles within the Ag matrix [34]. Understanding the observed XRD spectra requires accounting for this coherence between the two FCC phases in the calculation of the structure factor.

Due to the symmetry of the diffraction analysis, which allows one to reduce the problem to one dimension along the growth direction (GD), the simplest model for such a coherent binary nanocrystalline structure is that of a multilayer, as was shown for the Cu–Co system by Michælsen [18]. Then, the multilayer model refers not to a periodic stacking of continuous layers but to a homogeneous or pseudo-periodic distribution, in the GD, of aggregates in coherence with the matrix. In our case, with the periodicity in the GD of the aggregates being strongly disturbed, it is more convenient to use a bilayer for the calculation, the thicknesses of each layer being then distributed around a mean value.

An analytical expression for an ideal multilayer XRD pattern can be easily obtained [18, 30]. The various parameters allowing one to describe this structure are, for the two materials, the number and the interplanar separation distance of the diffracting planes, the atomic scattering coefficient and the number of bilayers (1 in our case). It is quite difficult to take into account the real effects of structural imperfections, which are certainly very important in that case, with the analytical approach. Moreover, the calculation of the XRD pattern of an imperfect superlattice can be performed by Monte Carlo simulation [31]. The definition of the structure is then completed by taking into account the following parameters:

(a) the atomic density of each phase;

(b) the deviation of the number of planes in each layer, which characterizes the size distribution of each of the aggregates in the GD;
(c) the interface half-thickness, which characterizes the interdiffusion between the two phases at interfaces and can be assimilated to grain boundaries.

In a first approximation, the atomic density of the layers is equal to that of the pure bulk materials and the atomic scattering factor is equal to the square of the atomic number. In the case of a binary alloyed phase, both values can be linearly extrapolated between those of the pure elements. In the present calculation, we considered the 'theoretical' structure to be a bilayer consisting of two types of layer corresponding to a stacking of the dense planes $\{hhh\}$ of two different FCC phases. One is a pure Ni phase, the other a homogeneous Ag–Ni solid solution. A Gaussian distribution, defined by its average root mean square, describes the distribution of the numbers of planes for each layer. To take into account the non-abrupt interface between the layers, we also considered an interdiffusion between them: interplanar distances vary linearly within two intermediate planes from that of the Ni phase to that of the Ag–Ni one.

Adjustments of the calculated patterns were carried out by varying five parameters: the number of planes n composing the two phases, the corresponding δn values and the interplanar distance d of the Ag–Ni solid solution (that of the pure Ni phase is constant, equal to the reference d_{111}-distance obtained for the pure bulk Ni sample). The uncertainty in the estimation of the different parameters can be estimated to about 10% for n and 0.001 nm for d.

Comparisons between the experimental and calculated x-ray diffraction patterns are given in figure 3(a) (as deposited) and figure 3(b) (annealed at 250 °C). The parameters deduced from the calculation are given in table 2. The agreement between the experimental and calculated patterns is good, although the model is oversimplified. In particular, the position and relative intensity of the shoulders with respect to the mean peak are correctly reproduced. The parameters characteristic of the Ag-rich phase remain constant during the thermal anneals. In contrast, the number of planes forming the pure Ni phase increases from 7 to 11 during

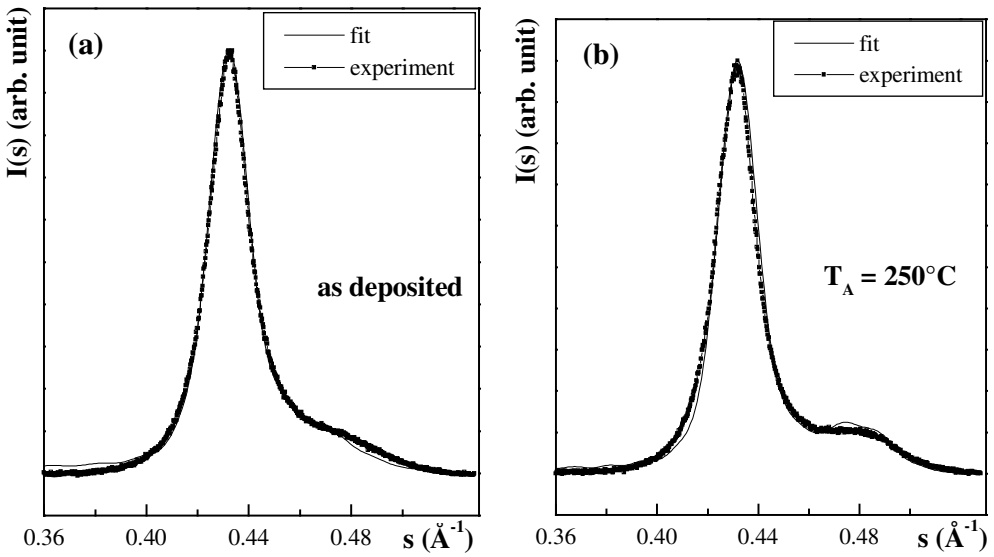

Figure 3. Modelling of the x-ray diffraction spectra measured for the $Ni_{0.35}Ag_{0.65}$ samples, as deposited (a) and annealed for ten minutes at 250 °C (b).

Table 2. Numerical values deduced from adjustments of the experimental x-ray diffraction pattern by a theoretical curve taking into account the structural coherence between phases, for the as-deposited and 250 °C annealed $Ni_{0.35}Ag_{0.65}$ deposited films. For each layer, one can determine: n, the number of reticular planes, δn, the deviation of the number n in a Gaussian distribution assumption, d, the interplanar distance, and D, the thickness.

Samples:	As deposited			250 °C		
Parameters:	n (δn)	d (nm)	D (nm)	n (δn)	d (nm)	D (nm)
Ag-rich layer	22 (8)	0.232	5.1 ± 0.5	22 (8)	0.232	5.1 ± 0.5
Pure Ni layer	7 (4)	0.2035	1.4 ± 0.2	11 (6)	0.2035	2.2 ± 0.2

the same treatment. The Gaussian distribution of the numbers of planes, characterized by the δn value, is rather large in all cases (δn being between around one-third and one-half of the n-value).

4.2. Asymmetric geometry: rocking curve

In order to quantify the disorientation ratio of the dense planes (111) of the silver-rich phase for the as-deposited sample, we performed rocking curve measurements (figure 4). The experimental points were adjusted by a Gaussian function: a full width at half-maximum value of 11° can be estimated for the peak, which shows partial texturing of the dense planes of the FCC silver-rich phase in the growth direction.

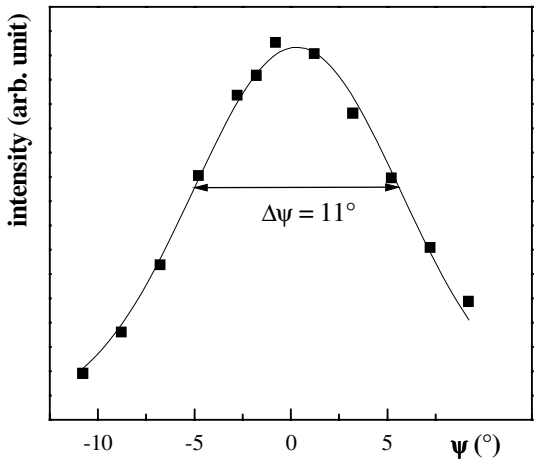

Figure 4. The Ag(111) rocking curve of the as-deposited $Ni_{0.35}Ag_{0.65}$ sample (■). Straight line: Gaussian fit.

This preferential orientation of the Ag-rich-phase dense planes has already been pointed out [14]. This observation was based on the absence of reflections ((200) and (311) for the Ag-rich phase) other than those attributed to the dense planes, in the symmetric geometry.

5. Discussion

5.1. Phase determination

The present interpretation of the x-ray diffraction patterns provides a consistent determination of the phases, the pure Ni and the Ag-rich solid solution, from the short-range-order (EXAFS) and long-range-order (XRD, ASAXS [16]) structural investigations. It is the combination of

these various techniques of structural characterization which supports such an interpretation of the XRD spectra. By themselves, the XRD spectra could not be interpreted unambiguously along the present lines without other structural information.

The Ni atomic concentration inserted in the Ag–Ni solid solution $C_{Ni}(Ag)$ can be calculated from the interplanar distances (table 2), by application of the Vegard law for both $Ni_{0.35}Ag_{0.65}$ films, as deposited and annealed at 250 °C. This concentration is estimated to be 7%. From the XAFS simulations, such a concentration can also be obtained. Assuming that the size effect has no influence on the Ni–Ag nearest-neighbour number [14], the Ni atomic fraction inserted in the Ag-rich phase can be calculated, $F_{Ni}(Ag) = N_{Ni-Ag}/12$. Starting from this fraction and from the global concentration $x = 0.35$, the Ni concentration in the Ag-rich phase is found to be constant for the samples studied and is estimated to be around 8%. Such a good agreement between the two calculated values allows us to determine the real Ni concentration in the Ag-rich phase around 7–8%. This turns out to be significantly smaller than the previous evaluation of 13% [14]. This previous determination was performed with a classical interpretation of the XRD pattern based on the location of the bottom of the peak (directly linked to an interplanar distance).

5.2. Shape and orientation of the nickel aggregates

The microstructure of the film and the shape of the crystallites are sensitive to the deposition conditions. The substrate temperature is of particular importance. At $T_{sub} = 77$ K, the growth of the film is mainly governed by random aggregation of the various atoms on the substrate, the surface diffusion being limited. The initial degree of intermixing between the two immiscible elements is then optimized. Calculations [35] performed by minimization of the free energy, in the general case of a strongly segregating binary system, homogeneous in the initial state, show then that the possible morphologies of the film are a layered structure and a combination of a column-like and a layered one. SAXS experiments [16] indicate that in the as-deposited $Ni_{0.35}Ag_{0.65}$ films, the Ni aggregates roughly consist of platelets, embedded in the silver matrix, homogeneously distributed in the films. Moreover, due to the geometry of the SAXS analysis (in the transmission mode), these two-dimensional aggregates are found to be preferentially orientated with their mean plane parallel to the surface. These results support the main hypothesis of our model, i.e. the pseudo-periodic stacking of Ni and Ag layers in the as-deposited state and the first stages of demixtion of the film.

Both types of crystallite, pure Ni and Ag-rich solid solution, are preferentially oriented with the dense planes parallel to the surface. This is deduced from the modelling of the symmetric XRD patterns and corroborated, for the Ag-rich phase, by asymmetric x-ray diffraction studies (however, the width of the rocking curve peak indicates a mosaic spread in this disordered phase).

5.3. Mean size of the aggregates

Different structural investigations allowed an estimation of the mean size of the pure Ni aggregates inserted in a silver-rich matrix for the $Ni_{0.35}Ag_{0.65}$ deposited films (figure 5): XAS (mean diameter $D_{Ni,XAS}$ or equivalent coherence length $L_{Ni,XAS}$—section 3), XRD (thickness D—section 4.1) and ASAXS [16] (mean radius $R_{Ni,ASAXS} \sim 0.6$ nm or, by analogy with equation (4), the equivalent length $L_{Ni,ASAXS} \sim 1$ nm). The main hypothesis made in estimating the size of the aggregates from the ASAXS and XAS results is their sphericity. This is not in contradiction with the 'lamellar microstructure' suggested by the modelling of the XRD spectra assuming a structural coherence between the two phases. The mean shape of the

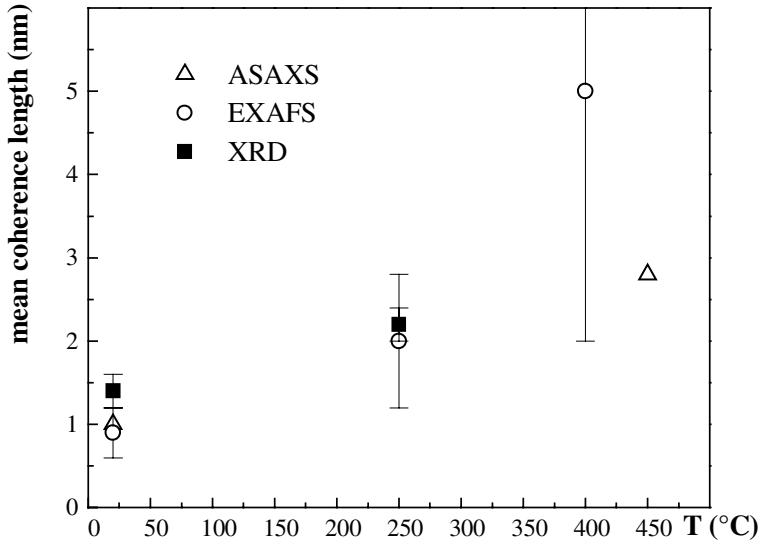

Figure 5. Mean equivalent coherence length (L, in nm) versus annealing temperature estimated from EXAFS, XRD and ASAXS measurements for $Ni_{0.35}Ag_{0.65}$ deposited materials.

various aggregates being almost geometrically isotropic [34], the size estimated by means of XRD, which corresponds to the mean coherence length in the GD, can be compared to that estimated by means of SAXS (perpendicular to the GD in the transmission mode) and XAFS (almost perpendicular to the GD due to the polarization effect).

Within the error bars, all the experimental values are equivalent: the mean equivalent coherence length is around 1.1 nm for the magnetic aggregates in the as-deposited state. With the annealing process, the mean size of these aggregates increases; the values obtained by the three methods are also very similar.

Moreover, two different treatments of the x-ray diffraction patterns, by Fourier analysis [14] and by the modelling described above (section 4.1), allowed an estimation of the size of the Ag-rich crystallites for the same sample. In both cases, the mean coherence length of the Ag-rich aggregates was found to be constant for these samples, with an estimated value of around 4.0 ± 0.5 nm with the first analysis process and around 5.1 ± 0.5 nm with the second one. These two values, although not overlapping within the error bars, are of the same order of magnitude. Finally, one can notice that the mean diameter of these crystallites roughly estimated from the full width at half-maximum value (≈ 0.02 Å^{-1}) is also around 5 nm, as obtained using the Scherrer formula.

5.4. Correlation with magneto-transport properties

The magnetic and transport properties of as-deposited and annealed Ni_xAg_{1-x} and Co_xAg_{1-x} alloys were discussed in an earlier paper [3]. The specific properties of the $Ni_{0.35}Ag_{0.65}$ alloys are examined and discussed here in more detail. The magnetoresistance curves, measured at various temperatures between 30 K and 300 K, are gathered in figure 6.

The MR curves of the as-deposited (figure 6(a)) and 250 °C annealed (figure 6(b)) samples are very similar. In these curves, the steep slope at relatively low fields and low temperature is associated with a change in the relative orientation of the magnetization in neighbouring magnetic aggregates. This is the same phenomenon as the GMR in magnetic multilayers

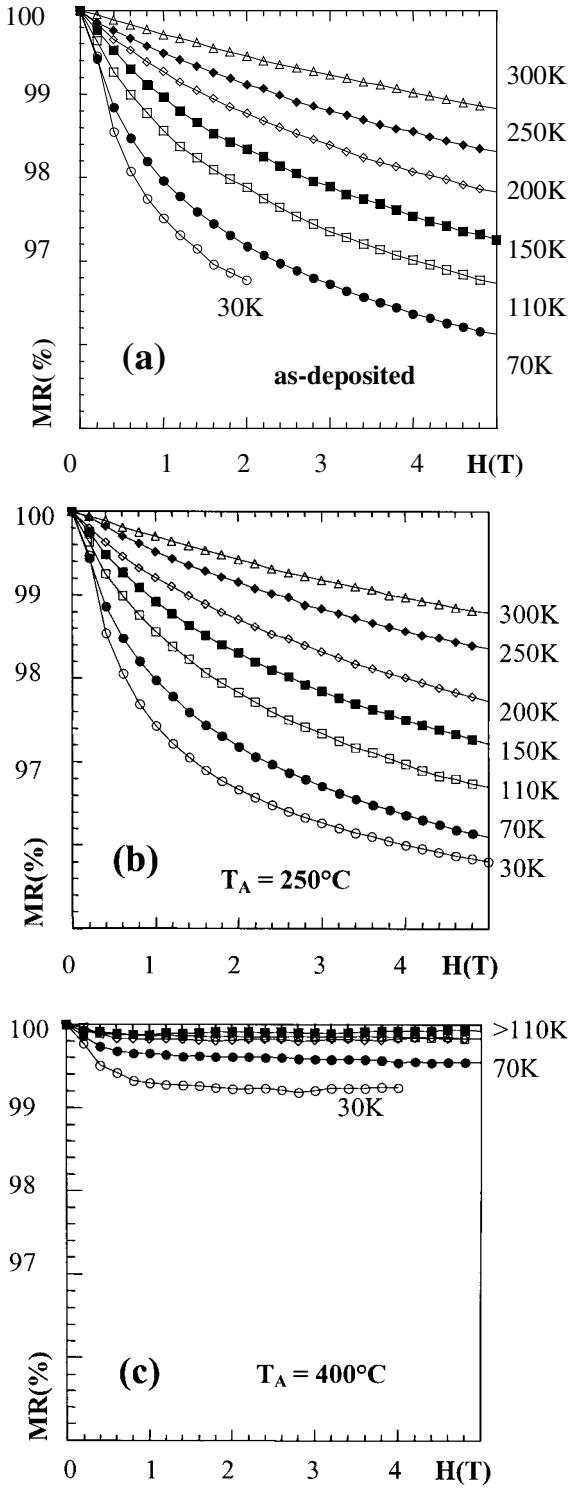

Figure 6. Magnetoresistance at various temperatures for as-deposited (a) and 250 °C (b) and 400 °C annealed (c) $Ni_{0.35}Ag_{0.65}$ samples.

caused by spin-dependent scattering of conduction electrons. In contrast, the high-field tail in the MR curves corresponds to very little change in the $M(H)$ curves [3]. This MR contribution is due to spin-disorder (SDMR) scattering. It is associated with the scattering of conduction electrons on interfacial magnetic fluctuations or small superparamagnetic aggregates. This contribution clearly dominates the GMR contribution in the as-deposited and 250 °C annealed samples, in which the magnetic Ni aggregates are very small.

Between the as-deposited and 250 °C annealed samples, significant variations in the structural and magnetic properties, but not in the transport properties, are observed. The size of the Ni aggregates slightly increases from 1.4 to 2.2 nm (from XRD measurements). This significantly changes the magnetic moment of the Ni precipitates and their internal ordering temperature [3], as well as the susceptibility of the heterogeneous alloy. However, the annealing does not change significantly the density of magnetic fluctuations between grains since the MR value due to these fluctuations is almost constant after the 250 °C anneal. The size of the Ni aggregates does not increase enough and the morphology and structure of the Ag-rich crystallites (which governed the distance between magnetic aggregates) remains unchanged.

Moreover, the tendency to form a Ni layered structure in the Ag-rich matrix certainly increases the ferromagnetic correlation between neighbouring particles. This reduces the GMR contribution by lowering the degree of antiparallel alignment between the magnetizations of neighbouring particles at low fields. This may explain the predominant role of SDMR in the as-deposited and 250 °C annealed samples.

For the 400 °C annealed sample (figure 6(c)), the high-field MR tails have disappeared. This means that magnetic fluctuations no longer play a significant role. This is certainly due to the demixing of the Ag-rich phase. There are no longer Ni atoms in the Ag matrix. The Ni/Ag interfaces are more abrupt. At 30 K, a GMR contribution is seen but it vanishes very quickly with increasing temperature. The MR is almost zero above 110 K. This strong decrease in MR amplitude cannot be explained by spin-flip scattering due to magnetic fluctuations since the latter have significantly decreased compared to those of the 250 °C annealed sample. We think that this is due to the complete loss of magnetic disorder between neighbouring particles. Due to the relatively soft properties of the Ni phase and to its layered structure, large ferromagnetic domains probably form in the Ni. In CoAg, we observed [3] that the MR amplitude was maximum after the 400 °C anneal, reaching 30% at 30 K in 2 T. An important difference between NiAg and CoAg alloys is the magnetocrystalline anisotropy in the metallic phase, much larger in Co than in Ni. In these alloys, the magnetic precipitates do not exhibit a well-defined texture. Therefore the uniaxial anisotropy axis within each precipitate can be considered as randomly oriented. If the anisotropy is large enough, as in cobalt, even if some ferromagnetic interactions exist between neighbouring precipitates due to the high concentration of the magnetic element, the anisotropy is sufficient to locally pull the magnetization in each precipitate towards its easy axis, thus generating a significant misalignment of the magnetization at low field. In contrast, if the anisotropy is weak, as in Ni, the ferromagnetic interactions between the Ni precipitates, reinforced because of the layered structure previously discussed, tend to create large ferromagnetic domains, the anisotropy not being strong enough to force the magnetic moment of the particles to locally deviate from the resultant direction. These domains can involve a very large number of particles, so the proportion of neighbouring particles not in parallel alignment at low fields is tiny, resulting in a small GMR amplitude. Since the anisotropy decreases quite rapidly with temperature, the size of the ferromagnetic domains increases rapidly, which may explain the disappearance of the MR above 110 K.

6. Conclusions

Long-range-order study of $Ni_{0.35}Ag_{0.65}$ thin films, as deposited and annealed at 250 °C, showed that the XRD patterns could be satisfactorily explained with a theoretical structural model where two phases, pure Ni and Ag–Ni solid solution, are distributed in a multilayered-like structure parallel to the surface and are partially structurally coherent. These thin films are composed of pure Ni aggregates statistically distributed through the Ag-rich matrix, developed during the deposition and/or the annealing processes. This structure organization produces a process of constructive interference between the amplitudes diffracted by each of the components. These interferences lead to the appearance of a diffraction peak in an intermediate location between the expected theoretical positions of the reflection under the dense planes of the two phases. This phenomenon is significant, and therefore visible, only if the size distribution of each phase is confined around a nanometre mean value.

The simulations of the XRD spectra are not unique. To be valid, such interpretation must be corroborated by other structural investigations performed on the same samples. In our case, this diffraction analysis yields results in good agreement with the EXAFS ones, the Fourier analysis of the XRD pattern and ASAXS. The estimates of the mean size of the pure Ni aggregates obtained from the three types of experiment are consistent. This size increases from around 1 nm in the as-deposited state to 3–5 nm upon a 400 °C anneal. Moreover, this interpretation of the XRD spectra has established the partial structural coherence between the Ni aggregates and the Ag-rich matrix. The relation between the magneto-transport properties and the microstructure characteristics of these $Ni_{0.35}Ag_{0.65}$ thin films was evident.

Acknowledgments

The authors wish to acknowledge Agnès Traverse for her considerable assistance on the EXAFS 13 beamline at LURE-DCI and Grzegorz Gladyszewski for the use of his program.

References

[1] Berkowitz A, Young A P, Mitchell J R, Zang S, Carey M J, Spada F E, Parker F T, Hutten A and Thomas G 1992 *Phys. Rev. Lett.* **68** 3745
[2] Xiao G, Jiang J S and Chien C L 1992 *Phys. Rev. Lett.* **68** 3749
[3] Mevel B 1997 *Thesis* Université Joseph Fourier, Grenoble
Nagamine L, Mevel B, Dieny B, Rodmacq B, Regnard J R, Revenant-Brizard C and Manzini I 1999 *J. Magn. Magn. Mater.* **195** 437
[4] Rodmacq B, George B, Vaezzadeh M and Mangin P 1992 *Phys. Rev.* B **46** 1206
[5] de Bœr F R, Boom R, Mattens W C M, Miedema A R and Niessen A K 1988 *Cohesion in Metals* ed F R de Bœr and D Pettifor (Amsterdam: Elsevier)
[6] Xu J, Herr U, Klassen T and Averbach R S 1996 *J. Appl. Phys.* **79** 3935
[7] Tung C Y, Lin H M, Gu J M and Lee P Y 1997 *Nanostruct. Mater.* **9** 117
Tung C Y, Gu J M, Lin H M, Hwu Y and Cheng N F 1997 *Nanostruct. Mater.* **9** 351
[8] Dimesso L and Hahn H 1998 *J. Appl. Phys.* **84** 953
[9] Tsaur B Y and Mayer J W 1980 *Appl. Phys. Lett.* **37** 389
[10] Weigang G, Hecht H and Von Minnigerode G 1995 *Z. Phys.* B **96** 349
[11] Van Ingen R P, Fastenau R H J and Mittemeijer E J 1994 *J. Appl. Phys.* **76** 1871
Krebs H U and Störmer M 1994 *Phys. Rev. Lett.* **72** 3116 (comment)
Van Ingen R P, Fastenau R H J and Mittemeijer E J 1995 *Phys. Rev. Lett.* **75** 3966 (reply to comment)
[12] Dahlgren S D, Patten J W and Thomas M T 1978 *Thin Solid Films* **53** 41
[13] Revenant-Brizard C, Regnard J R, Mimault J, Proux O, Dieny B and Mevel B 1997 *J. Physique Coll.* IV **7** C2 1111
[14] Proux O, Mimault J, Revenant-Brizard C, Regnard J R and Mevel B 1999 *J. Phys.: Condens. Matter* **11** 147

[15] Kubinski D J and Holloway H 1995 *J. Appl. Phys.* **77** 782
[16] Revenant-Brizard C, Simon J P, Regnard J R, Manzini I and Rodmacq B 1998 *J. Appl. Crystallogr.* **31** 783
[17] Mimault J, Proux O, Elkalkouli R and Girardeau T 1997 *J. Physique Coll.* IV **7** C2 1025
[18] Michælsen C 1995 *Phil. Mag.* A **72** 813
[19] Bimbault L, Badawi K F, Goudeau P, Mimault J and Proux O 1996 *J. Physique* IV **6** 43
[20] Girardeau T, Mimault J, Jaouen M, Chartier P and Tourillon G 1992 *Phys. Rev.* B **46** 7144
[21] Schrœder S L M 1996 *Solid State Commun.* **98** 405
[22] Mimault J, Faix J J, Girardeau T, Jaouen M and Tourillon G 1994 *Meas. Sci. Technol.* **5** 482
[23] McKale A G, Knapp G S and Chan S-K 1986 *Phys. Rev.* B **33** 841
[24] Michalowicz A 1991 *Soc. Fr. Chim.* 102
[25] Stern E A 1993 *Phys. Rev.* B **48** 9825
[26] Boscherini F, de Panfilis S and Weissmüller J 1998 *Phys. Rev.* B **57** 3365
[27] Borowski M 1997 *J. Physique. Coll.* IV **7** C2 259
[28] Naudon A, Slimani T and Goudeau P 1991 *J. Appl. Crystallogr.* **24** 501
[29] van Berkum J G M, Vermeulen A C, Delhez R, de Keijser T H and Mittemeijer E J 1994 *J. Appl. Crystallogr.* **27** 345
[30] Piecuch M and Nevot L 1990 *Metallic Multilayers (Materials Science Forum vols 59+60)* ed A Chamberod and J Hillairet (Zurich: Trans Tech Publications) p 93
[31] Gladyszewski G 1989 *Thin Solid Films* **170** 99
Gladyszewski G 1991 *Thin Solid Films* **204** 473
[32] Gurman S J, Binsted N and Ross I 1984 *J. Phys. C: Solid State Phys.* **17** 143
[33] Sánchez-Bajo F and Cumbrera F L 1997 *J. Appl. Crystallogr.* **30** 427
[34] Dieny B, Teixera S R, Rodmacq B, Cowache C, Auffret S, Redon O and Pierre J 1994 *J. Magn. Magn. Mater.* **130** 197
[35] Cserháti C, Szabó I A and Beke D L 1998 *Nanostruct. Mater.* **10** 195